

## 7. The effect of mechanical heterogeneity on plateau initiation - A modelling study with viscous-brittle media

Viscous-brittle analogue vise models, comprising two strong blocks that compress a weaker deformable domain, are employed to investigate critical factors for initiation of plateau-style tectonic deformation. The experiments focus on the role of mechanical heterogeneities in the lithosphere and specifically: 1) a critical lateral strength contrast between the strong “vises” and the intervening domain (e.g., more than twice the strength); 2) the presence of a decoupling horizon within the lower crust of the weak domain; 3) the degree of buoyancy of the lower crust; and 4) oroclinal bending. These parameters are shown to be first order features, which result in the formation of mountain ranges that enclose a flat basin, similar to geometries observed in nature (e.g., Andean and Tibetan plateaux). By further varying these parameters, for example by introducing additional decoupling horizons or decreasing the strength contrast between the strong blocks and the weak domain, the strain pattern at the surface remains that of a plateau-initiation setting, but has pronounced along-strike differences. Thus, some first order parameters have additional second order influence.

### 7.1. Introduction

Many driving factors are likely to play a role in the development of plateau orogens including crustal channel flow (e.g., Wdowinski and Bock, 1994a,b; Yuan et al., 2000; Husson and Sempere, 2003), climate (e.g., Masek et al., 1994; Horton, 1999; Lamb and Davis, 2003; Sobel et al., 2003), strength variations within the plates and their interface (e.g., Allmendinger and Gubbels, 1996; Lamb and Davis, 2003; Sobolev and Babeyko, 2005), mantle-driven processes (e.g., Kay and Kay, 1993; Allmendinger et al., 1997), changes in plate/indenter geometry (e.g., Gephart, 1994; Giese et al., 1999; Tassara, 2005), and convergence kinematics (e.g., Pardo-Casas et al., 1987; Somoza, 1998; Silver et al., 1998; Sobolev and Babeyko, 2005). Most of these studies on plateau formation focused on one potential driving factor that is able to account for the present-day strain pattern or the general orogen scale configuration. We suspect that several key conditions must be met early on in the initial system to allow the initiation of plateau growth (Oncken et al., 2006).

For the Tibetan plateau, Meyer et al. (1998) summarize the following conditions necessary for successful initial basin capture and subsequent plateau formation: 1) decoupling of crust and mantle produces a décollement, in which, 2) large, interconnected, coevally active thrusts root to produce, 3) broadly spaced parallel ranges that separate wide basins, 4) tectonic cut-off of river catchments that allows internal drainage of these basins, and 5) sedimentary infill from adjacent ranges, which finally leads to the smoothing of

relief and surface uplift (cf. Fig. 7.1).

The development of distinctly spaced high ranges that entail basin capture when supported by arid climate preventing the export of material have also been suggested to be crucial points for the Andean plateau (Sobel and Strecker, 2003; Sobel et al., 2003). Interestingly, the formation of spaced ranges entrapping a basin occurs on various length scales, from ~10 km in the Sierras Pampeanas and the Santa Barbara domain (Sobel et al., 2003; Mortimer et al., 2007) to the entire Altiplano (Elger et al., 2005) (Fig. 7.2).

The conditions for basin capture can be met by lithospheric buckling, where the wavelength of the periodic instabilities or buckle folds is determined by the vertical strength contrasts within the crust (e.g., Biot, 1961; Fletcher, 1974; Smith, 1975; Martinod and Davy, 1994; Burg and Podlachikov, 1999; Cagnard et al., 2006). However, previous

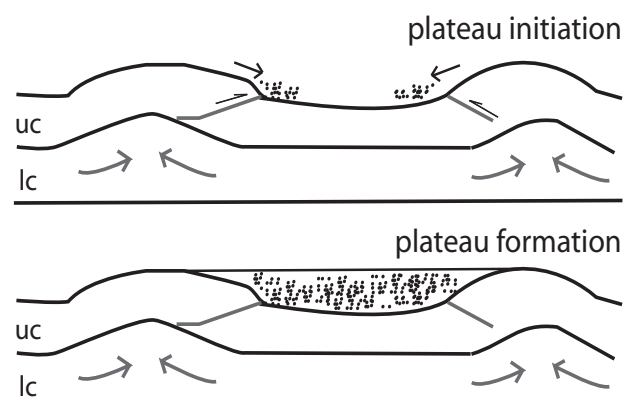


Fig. 7.1: Two evolutionary stages of plateaux include the plateau initiation, in which a basin is captured by two bounding ranges, and the plateau formation, which is successful when the basin has been drained, filled with sediments and uplifted.

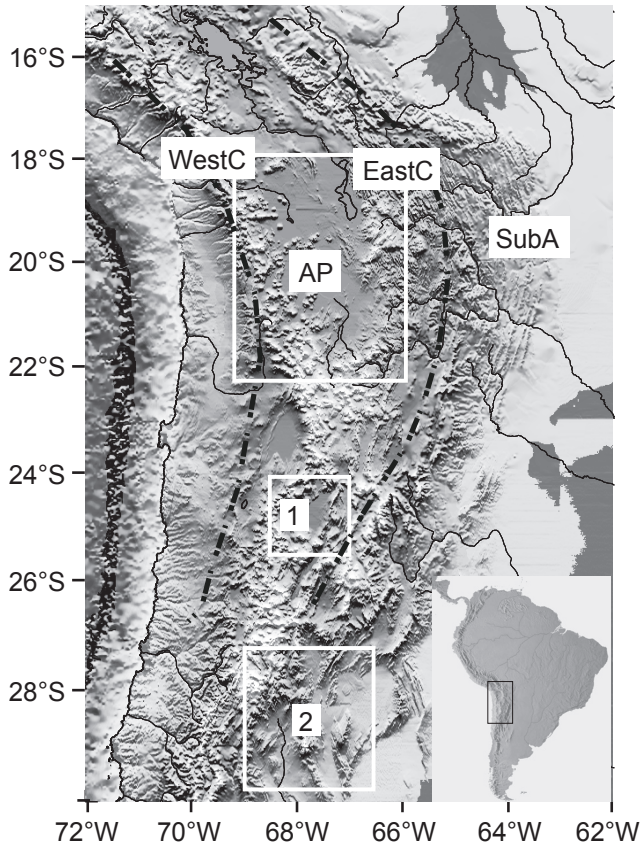


Fig. 7.2: Topomap of the study area of the Central Andes with main structural units; WestC: Pre- and Western Cordillera, AP: Altiplano plateau, EastC: Eastern Cordillera, SubA: Subandean fold-and-thrust belt (inset shows location in South America). Black dashed lines outline “vise” boundaries. White frames show locations of basins that have been preserved in between mountain ranges and internally drained (AP: Altiplano, 1: Puna, 2: Sierras Pampeanas).

studies have several limiting factors with respect to natural examples of plateau initiation: 1) the crust is horizontally homogeneous and strength contrasts exist only vertically, 2) strain localization does not occur in a similar fashion to that in nature, where it is guided by weak zones that are more prone to strain accumulation than others, 3) lithospheric buckles often occur instantaneously and coevally, and cannot explain the chronological evolution of mountain ranges and entrapped basins observed in natural systems, and 4) they cannot account for processes operating at distinctly different spatial length scales.

In this paper we investigate the role of mechanical heterogeneity in the lithosphere on basin capture and the initiation of plateaux, consisting of a combination of both vertical and horizontal physical contrasts (strength and density). Thus we aim to address some limitations of previous models, and to investigate the role of coupled parameters that can explain the initiation of plateaux, which are both comparable to nature and

have the potential to develop a plateau thereafter. These include lateral strength contrasts between the strong “vises” and the intervening domain, decoupling horizons within the lower crust of the weak domain, degrees of buoyancy of the lower crust, and oroclinal bending.

We accomplish this by viscous-brittle analogue experiments following previous numerical and laboratory vise simulations (Ellis et al., 1998; Cruden et al., 2006), in which a weak domain is compressed in between two strong blocks. Particle imaging velocimetry (cf. Adam et al., 2004) enables high-resolution monitoring of the evolution of strain in space and time, and the development of 3D topographic relief. Thus we can compare our models to natural examples at the orogen scale, and are also able to detect variations on smaller scales.

## 7.2. Experimental design

### 7.2.1. Experimental procedure

The model set-up is similar to previous analogue vise models (Cruden et al., 2006), in which two strong blocks (“vise 1” attached to the advancing piston, and “vise 2” on the opposite immobile side) compress a weak domain. Both the vises and the intervening domain are composed of brittle upper crust, a viscous lower crust and a viscous mantle lithosphere floating isostatically on the asthenosphere (Fig. 7.3). The boundaries to the sides of the box are closed to avoid lateral extrusion of the model.

One piston is advanced into the model at a constant rate during the experiment. The contacts of vise and piston, vise and weak domain, vise and tank wall, and weak domain and tank wall are no-slip boundaries. The upper boundary is a free surface.

### 7.2.2. Scaling

All scaling factors are dimensionless ratios of model to nature (Table 7.1). The length scale ratio yields  $L^* = l_{\text{mod}}/l_{\text{nat}} = 3.75 \times 10^{-7}$ , as we use a model crustal thickness  $l_{\text{mod}} = 1.2$  cm, which corresponds to 32 km in nature. The density ratio  $\rho^* = \rho_{\text{mod}}/\rho_{\text{nat}}$  is 0.326 given by a mantle lithosphere density of 3000 kg/m<sup>3</sup> and a model density of 980 kg/m<sup>3</sup>. The gravity for the models is the same as in nature, so that  $g^*$  is 1. Thus, the stress scaling factor  $\sigma^* = L^* \rho^* g^*$  yields  $1.2225 \times 10^{-7}$ .

The viscosity ratio  $\eta^* = \eta_{\text{mod}}/\eta_{\text{vat}}$  yields a factor of  $5 \times 10^{-18}$  Pa s, if we assume  $5.9 \times 10^{21}$  Pa

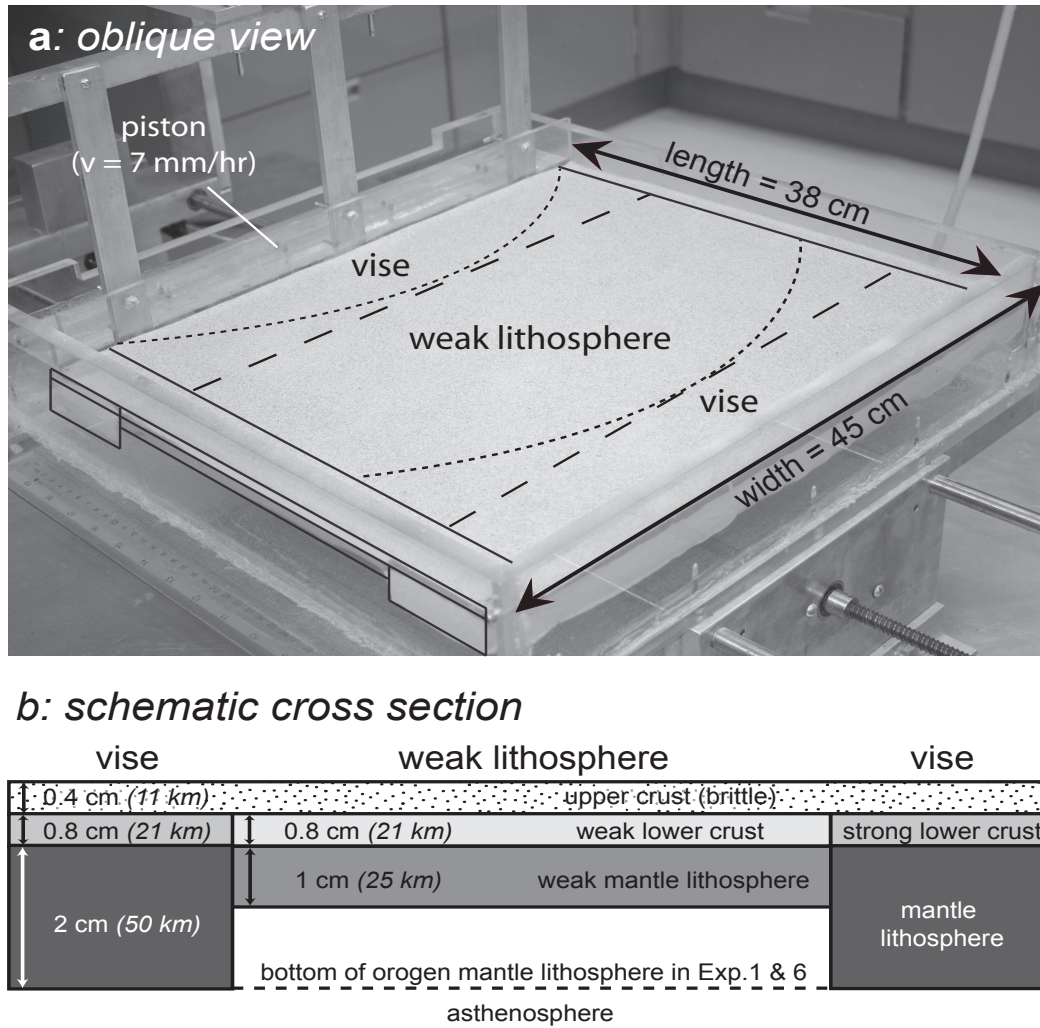


Fig. 7.3: a) Photograph of experimental set-up. The shape of the “vises” is either curved or straight. Tank dimensions are 46 cm x 45 cm x 10 cm, but the experimental set-up surface is only 38 cm (length) x 45 cm (width).

b) The thicknesses for each layer are given with the natural equivalents (in italics). In two experiments (Exp. 1 and Exp. 6), the mantle lithosphere of the weak domain has the same thickness as the vise mantle lithosphere (both 2 cm).

s as viscosity for the natural mantle lithosphere of the weak domain, which we model with material that has a viscosity of  $2.95 \times 10^4$  Pa s at an experimental strain rate of  $2.44 \times 10^{-5} \text{ s}^{-1}$ . Further, we obtain the duration of our model runs  $t^* = \eta^*/\sigma^*$  with  $t_{\text{mod}}/t_{\text{nat}} = 5 \times 10^{-18}/(0.326 \times 3.75 \times 10^{-7}) = 4.1 \times 10^{-11}$ . For our deformational system to develop we assume a duration of  $t_{\text{nat}} = 40 \text{ Ma} (= 3.504 \times 10^{11} \text{ h})$  which gives  $t_{\text{mod}} = 14.3 \text{ h}$ .

Of further interest is  $\varepsilon^{\text{dot}*} = \sigma^*/\eta^*$  which results in  $2.44 \times 10^{10}$ , where  $\varepsilon^{\text{dot}*}$  is the dimensionless ratio for strain rate. Therefore natural strain rates on the order of  $10^{-15} \text{ s}^{-1}$  are scaled with model strain rates of  $\varepsilon^{\text{dot}}_{\text{mod}} = 2.44 \times 10^{-5} \text{ s}^{-1}$ . Velocities are scaled by  $V^* = \varepsilon^{\text{dot}*} L^*$ . Thus  $V_{\text{mod}}/V_{\text{nat}}$  is given by  $2.44 \times 10^{10} \times 3.75 \times 10^{-7}$  which yields  $V^* = 9146.3$ . Assuming an average amount of shortening in nature of about 280 km over 40 Ma, the shortening rate is 7 km/Ma ( $8 \times 10^{-4} \text{ mm/h}$ ), and we obtain  $V_{\text{mod}} = 7 \text{ mm/h}$ . To verify the values for velocity and time, we use

$V^* = L^*/t^*$ , which is  $3.75 \times 10^{-7}/4.1 \times 10^{-11} = 9146.3$ . A total experimental run of 14.3 hours results in about 10 cm of piston convergence and a bulk shortening of 27.7 %. All scaling parameters are summarized in Table 7.1.

### 7.2.3. Materials and model construction

Variations in viscosity and density of viscous laboratory materials are accomplished by adding Harbutt’s plasticene, bouncing putty, low-viscosity silicone or granular fillers like 3M Z-lights ceramic microspheres, and 3M Scotchlith Glass Bubbles to transparent Polydimethylsiloxane (PDMS) (for details refer to Cruden et al., 2006). The rheological properties were measured for all viscous mixtures using a TA Instruments AR1000 rheometer over a broad range of stresses at ambient room temperature. Strength profiles of both weak lithosphere and strong vises are presented in Figure 7.4.



Table 7.1. Scaling parameters

Parameter	Equation	Nature	Model	Scaling factor
<i>Initial Thickness</i>				
	$L_{mod}/L_{nat}$			$L^* = 3.75 \times 10^{-7}$
upper crust		10.7 km	0.4 cm	
lower crust		21.3 km	0.8 cm	
mantle lith. (weak)		(26.7 km or) 53.4 km	(1 cm or) 2 cm	
mantle lith. (vise)		53.4 km	2 cm	
mantle asthenosphere		120.2 km	4.5 cm	
<i>Density</i>				
	$\rho_{mod}/\rho_{nat}$			$\rho^* = 0.326$
upper crust		2600 kg/m <sup>3</sup>	850 kg/m <sup>3</sup>	
lower crust (weak)		2480 kg/m <sup>3</sup> ; 2900 kg/m <sup>3</sup>	810 kg/m <sup>3</sup> ; 950 kg/m <sup>3</sup>	
lower crust (vise)		2900 kg/m <sup>3</sup>	950 kg/m <sup>3</sup>	
mantle lith. (weak)		3000 kg/m <sup>3</sup>	980 kg/m <sup>3</sup>	
mantle lith. (vise)		3030 kg/m <sup>3</sup>	990 kg/m <sup>3</sup>	
mantle asthenosphere		not scaled	1000 kg/m <sup>3</sup>	
<i>Viscosity</i>				
	$\eta_{mod}/\eta_{nat}$			$\eta^* = 5 \times 10^{-18} \text{ Pa s}$
lower crust (weak)		3 - 4.2 x 10 <sup>21</sup> Pa s	1.5 - 2.1 x 10 <sup>4</sup> Pa s	
lower crust (vise)		9 x 10 <sup>21</sup> Pa s	4.5 x 10 <sup>4</sup> Pa s	
mantle lith. (weak)		5.9 x 10 <sup>21</sup> Pa s	2.95 x 10 <sup>4</sup> Pa s	
mantle lith. (vise)		3.6 x 10 <sup>22</sup> Pa s	1.83 x 10 <sup>5</sup> Pa s	
mantle asthenosphere		not scaled	0.89 x 10 <sup>-3</sup> Pa s	
low-viscosity layer		~10 <sup>16</sup> -10 <sup>17</sup> Pa s	10 <sup>1</sup> -10 <sup>2</sup> Pa s	
<i>Gravity</i>				
	g	9.81 m s <sup>-2</sup>	9.81 m s <sup>-2</sup>	$g^* = 1$
<i>Strain rate</i>				
	$\dot{\epsilon}^{dot*} = \sigma^*/\eta^*$	10 <sup>-15</sup> s <sup>-1</sup>	2.44 x 10 <sup>-5</sup> s <sup>-1</sup>	$\dot{\epsilon}^{dot*} = 2.44 \times 10^{10}$
<i>Time</i>				
	$t^* = \eta^*/\sigma^*$	40 Ma	14.3 h	$t^* = 4.1 \times 10^{-11}$
<i>Convergence rate</i>				
	$V^* = L^*/t^*$	7 mm/yr	7 mm/h	$V^* = 9146.3$
<i>Stress</i>				
	$\sigma^* = \rho^* g^* L^*$			$\sigma^* = 1.2225 \times 10^{-7}$

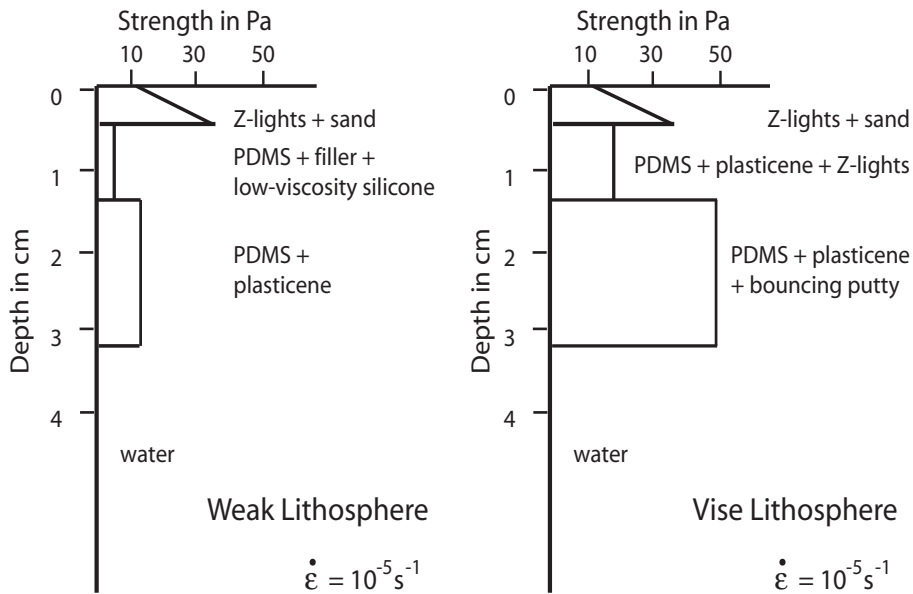


Fig. 7.4: Strength profiles for material mixtures used in both the “weak” lithosphere (left) and the strong “vise” lithosphere (right). For densities and viscosities of materials confer Table 7.1.



## 7. The effect of mechanical heterogeneity on plateau initiation

Table 7.2. Initial characteristics and resulting patterns of experiments.

	Initial Characteristics	Resulting pattern	Strain localization at % of bulk shortening
Exp. 1	Straight vises, non-buoyant lower crust, 2 cm mantle lithosphere in weak domain	cross-shaped (broad)	10 %
Exp. 2	Straight vises, buoyant lower crust, 1 cm mantle lithosphere in weak domain	cross-shaped (narrow)	4-6 %
Exp. 3	Curved vises, buoyant lower crust, 1 cm mantle lithosphere in weak domain	horizontal Phi (narrow)	5 %
Exp. 4	Curved vises, non-buoyant lower crust, 1 cm mantle lithosphere in weak domain	horizontal Phi (broad)	11.5 %
Exp. 5	Curved vises, non-buoyant lower crust, 1 cm mantle lithosphere, additional low-viscosity horizon	horizontal Phi (broad)	11.5 %
Exp. 6	Curved vises, non-buoyant lower crust, 2 cm mantle lithosphere in weak domain	horizontal Phi (broad)	11.5 %
Exp. 7	Curved, small vises, non-buoyant lower crust, 1 cm mantle lithosphere in weak domain	other	11 %
Exp. 8	Curved, small vise 1, straight vise 2, non-buoyant lower crust, 1 cm mantle lithosphere	mix of cross-shaped and horizontal Phi	12 %
Exp. 9	Curved vises, buoyant domain within non-buoyant domains, 1 cm mantle lithosphere	other	13 %

To ensure that the system is not coupled to mantle flow (e.g., by drag from below), we use water as our model asthenosphere. The viscosity of the asthenosphere is therefore underestimated, but the role of this layer in our experiments is solely to provide isostatic equilibrium.

After thorough mixing, each layer is allowed to relax in a frame to remove air bubbles. Layers of the mantle lithosphere, both of the vises and the weak domain, are later assembled together in a larger frame and allowed to flow into contact. Next, the layers of the lower crust are placed on top and allowed to settle. Finally, the large frame containing all the viscous units is put into a freezer, so that the layers can be placed on the water as one solid block.

After warming up to ambient room temperature and isostatic readjustment, a granular upper crust composed of sand and Z-lights is sieved on top of the model. To minimize boundary effects within the system, an additional buffer layer of pure PDMS is introduced along the sides orthogonal to the piston, on which no granular material is placed.

### 7.2.4. Dimensions of the experimental set-up

The experimental tank is 46 x 45 x 10 cm<sup>3</sup> (length x width x depth) (Fig. 7.3). Convergence is in the direction of length. Due to the position of

the piston, the total length of the experiment is 38 cm, of which each vise makes up 7 cm and the weak domain has a length of 24 cm. The width of each unit is 41 cm with an additional 2 cm on each side to avoid boundary effects. The depth of the piston corresponds to the bottom of the mantle lithosphere, thus only the viscous layers are pushed, and the asthenospheric mantle flows freely below the piston. Thicknesses for the vise are the following: 2 cm of mantle lithosphere, 0.8 cm of lower crust and 0.4 cm of upper crust; and for the weak domain: 1 cm of mantle lithosphere, 0.8 cm of lower crust and 0.4 cm of upper crust (Table 7.1). In two experiments, the mantle lithosphere of this domain is also 2 cm (Exp. 1, 6, Table 7.2).

For experiments with curved vises, the one attached to the piston has a maximum length of 7 cm at its center point decreasing to the sides, whereas the vise on the other immobile side has a minimum length of 7 cm in its center point increasing in length towards the sides to reach 14 cm. The curvature angle is about 20° (Fig. 7.3).

### 7.2.5. Monitoring technique

In order to quantify the instantaneous horizontal velocities and vertical displacements of the model surface, all experiments are monitored by “particle imaging velocimetry” (PIV) (cf. Adam et al., 2004). The surface is imaged by two

stereoscopic cameras, which are calibrated (3D volume calibration) before each experiment to obtain a mapping function. This function is used for the error evaluation, which is on the order of  $10^{-1}$  pixel. One pixel equals 0.33 mm, so the error is one order of magnitude smaller than the size of a single sand grain ( $\sim 400 \mu\text{m}$ ). Digital images are taken every five minutes, which equals 0.6 mm of shortening at a motor speed of 7 mm/h.

Data processing further includes the calculation of digital elevation models for each of the stereo image pairs, which serve as the base for the subsequent computation of the observed velocity field. This is achieved by cross-correlation of sequential images by the commercial software LaVision DaVis (for details refer to Adam et al., 2004). The velocity field is then used to compute incremental and cumulative strain gradients in multiple directions (e.g., in  $E_{xx}$ ,  $E_{yy}$ ,  $E_{xy}$ ).

### 7.3. Experimental results

#### 7.3.1. Tested parameters

The initial set-up generally follows the model in Figure 7.3 depending on the implementation of the following parameters, which are based on features of the Central Andes: a) the geometry of the vises (oroclinal bend of the Central Andes, cf. Fig. 7.2), b) an additional low-viscosity horizon in the lower crust (zone of partial melt beneath the Andean plateau), c) lateral strength contrasts between two stronger units compressing a weaker domain (vises: the Andean forearc as the “pseudo-indenter”, Victor et al., 2004; Tassara, 2005; and the strong Brazilian Shield, e.g., Sobolev and Babeyko, 2005), and d) the density profile (studying the two possible end members of density variations due to, e.g., the presence of partial melt or delamination processes).

Figure 7.5 presents the resulting strain patterns of all nine experiments depending on the changed parameter combinations. The upper row shows the different tested geometries of the vises, which are combined with various characteristics given on the left hand side (buoyancy, decoupling layers, and mantle lithosphere thickness). The initial characteristics and the resulting strain patterns are also summarized in Table 7.2 and are described in more detail below.

#### 7.3.2. Strain patterns

The resulting finite strain patterns can be grouped into 1) “cross-shaped” patterns (Exp. 1,

2); 2) “horizontal phi”-patterns (Exp. 3, 4, 5, 6); and 3) other patterns (Exp. 7, 8, 9).

##### 7.3.2.1. Cross-shaped pattern

The first group (Exp. 1 and 2) is characterized by a final strain pattern that resembles a saltire, as the structures cross in the center of the weak domain at a very low angle, and move outwards to both sides (Fig. 7.5a+b). No plateaux are initiated, as the anticlinal hinges do not capture an undeformed area in between (Exp. 1, 2, Fig. 7.5a+b). This is possibly due to the limiting effect of the side walls of the tank, which might not happen when the experimental set-up was larger.

Both experiments have straight vises on both sides; the lower crust in Exp. 1 (Fig. 7.5a) is non-buoyant with respect to the upper crust, and buoyant in Exp. 2 (Fig. 7.5b). In Exp. 1, the first thrust develops about 2 cm inward from vise 1 in the weak domain after about 10% of bulk shortening. At about 13% of bulk shortening eight thrusts begin to develop coevally, and are distributed within the weak domain with a spacing of 2-6 cm. Localization mostly initiates in the center of the model, from where thrusts propagate laterally closer to the vises. With increased shortening, thrusts develop hanging wall anticlines that gain in elevation. Strain is accumulated solely within these structures.

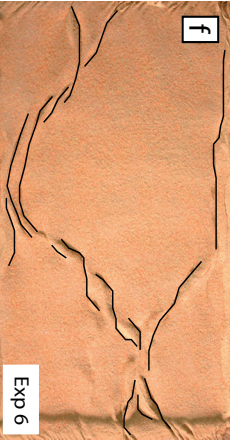
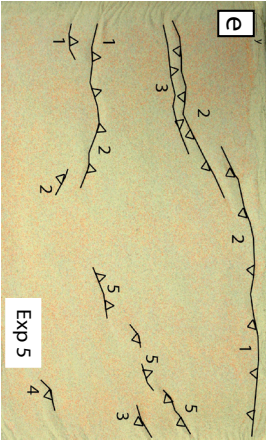
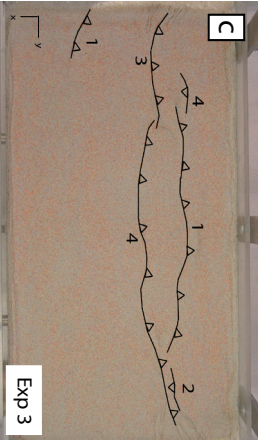
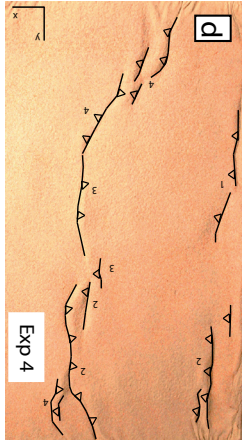
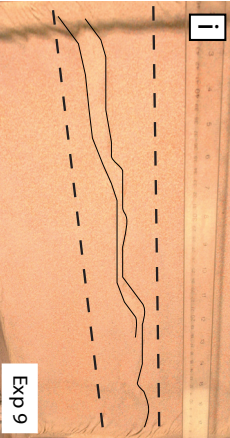
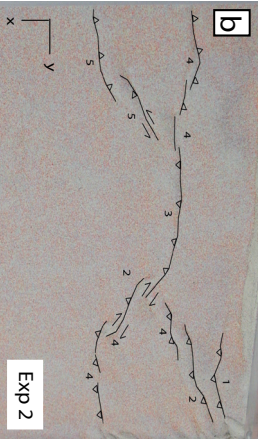
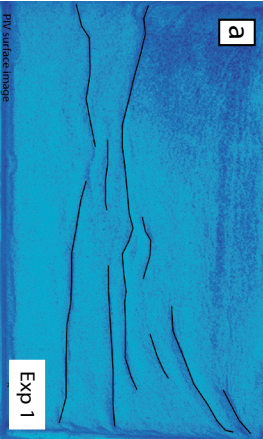
In Exp. 2, a first set of three en-echelon structures develops from the piston close to the side walls inwards towards the front wall at 4-6% of bulk shortening. Subsequently, a major structure develops within the center, coevally with another set of en-echelon faults that localizes from the center outwards towards the first en-echelon set. After 9% of bulk shortening, the main structure in the center extends towards the sides near the back wall, followed by another en-echelon set towards the front wall. After about 14% of bulk shortening, the cross-shaped strain pattern remains unchanged and accumulates all subsequent strain.

Figure 7.6 shows topographic profiles across the system for experiments 1 and 2. They do not exhibit flat and relatively undeformed areas that are entrapped by anticlinal hinges.

##### 7.3.2.2. Phi pattern (plateau-initiation)

Characteristic for the plateau-initiation settings is the development of two anticlinal

7. The effect of mechanical heterogeneity on plateau initiation

Thick mantle lith	LVL	Buoyant lc	Non-buoyant lc	
 <p>Exp 6</p>	 <p>Exp 5</p>	 <p>Exp 3</p>	 <p>Exp 4</p>	<div style="display: flex; justify-content: space-around; align-items: center;"> <div style="border: 1px solid black; padding: 5px; text-align: center;">             vise 1 weak lithosphere vise 2           </div> <div style="text-align: center;"> <p><b>convergence</b></p> <p>↑</p> </div> <div style="border: 1px solid black; padding: 5px; text-align: center;">             vise 1 weak lithosphere vise 2           </div> </div>
 <p>Exp 9</p>	<p style="text-align: center;">other (cf. text)</p>	 <p>Exp 2</p>	 <p>Exp 1</p>	<div style="display: flex; justify-content: space-around; align-items: center;"> <div style="border: 1px solid black; padding: 5px; text-align: center;">             vise 1 weak lithosphere vise 2           </div> <div style="border: 1px solid black; padding: 5px; text-align: center;">             vise 1 weak lithosphere vise 2           </div> <div style="border: 1px solid black; padding: 5px; text-align: center;">             vise 1 weak lithosphere vise 2           </div> </div>



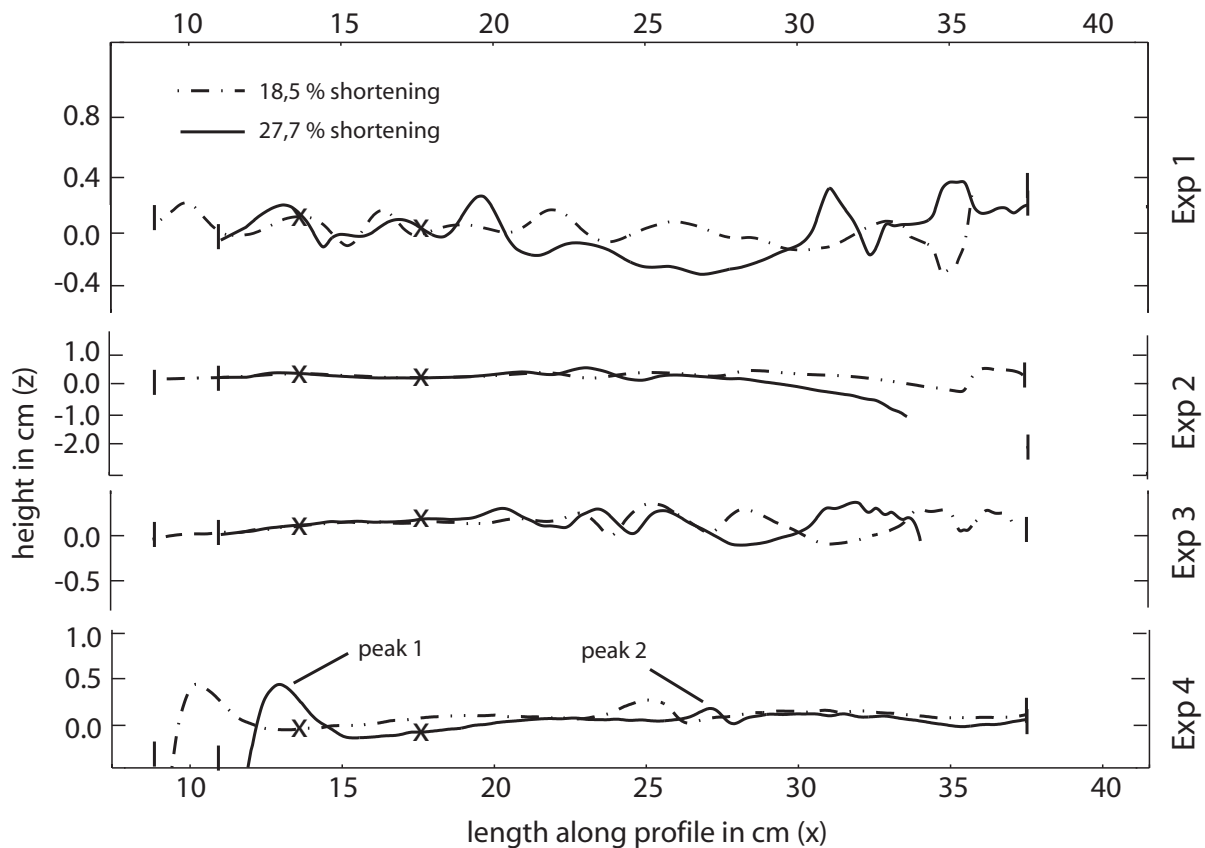


Fig. 7.6: Topographic profiles of Experiments 1, 2, 3 (non-plateau style) vs. Experiment 4 (plateau-initiation setting). For each of the experiments the elevation is plotted of one central profile (location: profile 2, Fig. 7.9a) after 18.5% shortening (stippled line), and 27.7% shortening (total amount, solid line). The plateau-initiation setting (basic setting, Exp. 4) is characterized by two final peak ridges (at 13 cm and at 27 cm) which bound a wide, flat area. Note the breaks on the y-axis, and the differences in vertical exaggeration. Crosses mark the approximate position of the boundary of vise 1 and the weak domain.

hinges with a general strike orthogonal to the direction of convergence with a slight concave curvature that bound a flat and undeformed area. This area will subsequently be part of the plateau formation process including internal drainage, uplift and sedimentary infill. The final strain pattern resembles a “phi” turned 90°.

All experiments (Exp. 3-6, Fig. 7.5c-f) have curved vises on both sides, with a convex shaped vise 1 (attached to the piston wall) and a concave shaped vise 2. Apart from Exp. 3 (Fig. 7.5c), the lower crust is non-buoyant with respect to the upper crust (Table 7.2). Exp. 4-6 (Fig. 7.5d-f) further differ from each other due to the presence of a low-viscosity silicone layer in the lower crust (Exp.

5, Fig. 7.5e), ~2 mm below its surface, simulating a zone of partial melt. This position at a depth of ~6 mm corresponds to a zone of partial melt a depth of ~16 km in nature. The weak mantle lithosphere in Exp. 6 (Fig. 7.5f) has the same thickness as that of the vises (2 cm).

In the experiment with buoyant lower crust (Exp. 3, Fig. 7.5c) strain localization begins already at 5% of bulk shortening, when the first structure develops in the center of the weak lithosphere, ~4 cm from the boundary of vise 1. The fault extends to the sides up to a distance of about 10 cm. Another fault develops on both sides 3 cm further towards vise 2, and extends from the tip of the first fault closer to the sides. Another main structure develops in the center of the weak domain, at a distance of about 8 cm from the first main feature. This last structure develops after 7% of bulk shortening, and has a similar lateral extent as the first thrust.

In contrast, strain localization in experiments with non-buoyant lower crust begins much later (e.g., after 11.5% of bulk shortening, cf. Table 7.2). In Exp. 4 (Fig. 7.5d) strain first localizes

Fig. 7.5 (left): Photographs of the experimental surfaces after 27.7% of bulk shortening (convergence from top to bottom). The final area has a size of 27.5 cm (x-direction) and 45 cm (y-direction). Thrusts are partly numbered according to their appearance. The upper row of experiments shows the configurations with non-buoyant lower crust and the respective geometry of the vises (curvature and size) visible above. Rows below show experiments with a buoyant lower crust, a low-viscosity layer and a thick mantle lithosphere (a. to i. mark Experiments 1 to 9). Further details on experimental set-up and structural development in-text.

along faults close to the piston within the weak domain both in the center and from the sides towards the center. These faults later interconnect. More thrusts develop, which extend across to the other side wall (until 27.7% of bulk shortening). The timing of strain localization and the position of both the thrusts and the undeformed area in Exp. 5 and 6 is similar to Exp. 4. However, instead of forming a more or less continuing range with a slight curvature, the curvature becomes much more pronounced as the faults form step-over zones instead of interconnecting with each other in Exp. 6 (Fig. 7.5f). They curve strongly inwards towards the side walls, so that the two ranges almost merge. The area that has been left undeformed in between these two features is wider than in Exp. 4 (Fig. 7.5d) and Exp. 5 (Fig. 7.5e).

The topographic profile of Exp. 4 (Fig. 7.6) clearly shows that plateau-initiation settings are characterized by anticlinal hinges that bound a flat and undeformed area in between. This is less obvious for the profile of Exp. 3, in which the basin area is very narrow.

### 7.3.2.3. Other patterns

The other experiments do not develop either of the two patterns (Exp. 8, 9, Fig. 7.5h+i), or display both patterns at the same time (Exp. 7, Fig. 7.5g).

Exp. 7 (Fig. 7.5g) has a curved vise 1 that is 30 cm wide (about 50°), and a straight vise 2 that extends all across the width of the box. Lower crust is non-buoyant. Thrusts develop at ~12% of bulk shortening (from one side towards the middle in the center of the weak domain), at ~18% of bulk shortening (in the center of the weak domain develops closer to the piston), and thereafter (extending further to the sides connecting to previous faults to form a small step-over zone). The final pattern resembles a mixture of the cross-shape and “phi”-pattern: along-strike of the set-up, the cross-shape pattern dominates from the sidewalls to the boundaries of vise 1, whereas a very narrow “phi” pattern occurs from one vise boundary to the other (Fig. 7.5g).

Exp. 8 (Fig. 7.5h) has a convex vise 1 and concave vise 2, but vises do not extend to the sides as they are only 30 cm wide (instead of 41 cm). Lower crust is non-buoyant. After ~11% of bulk shortening, thrusts localize strain in the center close to the front wall, and about ten faults of various sizes extend to the sides in en-echelon

patterns that step back close to the back wall. The final pattern therefore resembles a single curve (Fig. 7.5h).

Exp. 9 (Fig. 7.5i) has a convex vise 1 and a concave vise 2. Its lower crust is non-buoyant with respect to the upper crust for the first 7 cm inwards from vise 1, followed by 10 cm of buoyant crust, and another 7 cm of non-buoyant crust, so that two lateral density contrasts are present within the lower crust (with the two end member densities of 0.81 and 0.94 g/cm<sup>3</sup>). Strain localizes in the center of the experiment in the middle of the buoyant domain after ~13% of bulk shortening. These thrusts subsequently interconnect and develop step-over zones (Fig. 7.5i).

### 7.3.3. Deformation mode

The deformation modes within the viscous layers (pure shear, homogeneous thickening) are different to that observed in the granular upper crust (strain localized along faults). However, faults in the brittle crust localize within the same vertical column as lower crustal antiform-synform structures.

Based on the analysis of subsequent PIV images and the finite deformation of the viscous layers observed in model cross sections, we propose the following sequence of structural evolution (Fig. 7.7): 1) strain accumulates by pure shear of the viscous layers while deformation of the upper crust is restricted to the piston and back walls of the box; 2) strain eventually localizes as thrusts in the upper crust; 3) thrusting then creates accommodation space, so that the ductile lower crust can thicken below; and the upper crust further bulges above the thickening lower crust; 4) sedimentation from the hanging wall onto the footwall results in a sedimentary load that causes formation of footwall synclines in the lower crust; and 5) the lateral strength contrast between the sediment filled syncline and adjacent viscous crust causes thrusting on the other side of the syncline (viz., Cagnard et al., 2006).

Newtonian viscous layers (or nearly Newtonian fluids) deform homogeneously and therefore do not exhibit strain localization. It could be argued that if random heterogeneities were present within the viscous layers, they could be responsible for the formation of anticlines (by upward bulges of the lower crust), which would in turn cause strain to localize in the upper crust directly above the bulges. However,

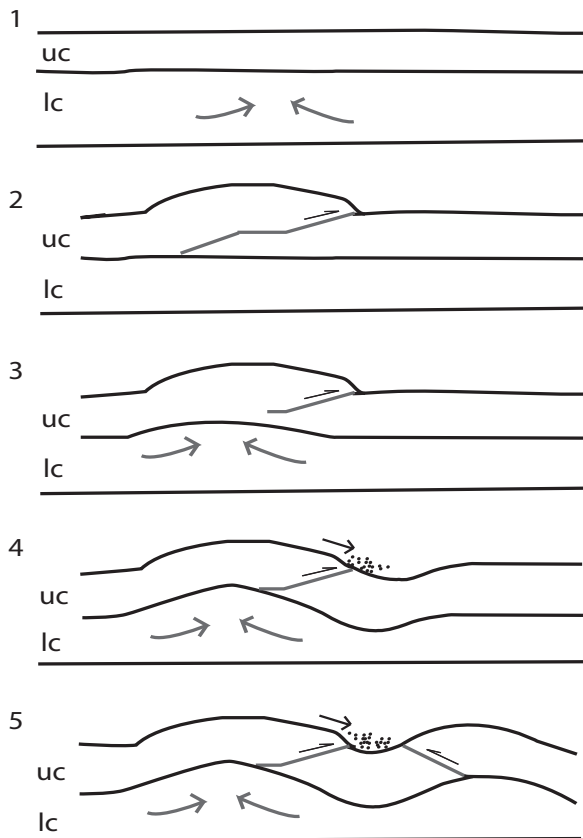


Fig. 7.7: Evolution of structures within the upper (uc) and lower crust (lc) indicates decoupling of deformation of both layers. See text for further explanation.

such a mechanism relies solely on the random distribution of heterogeneities (possibly due to mixing of material), which in turn would not be expected to develop the recurrent patterns in our experiments (e.g., the cross-shaped or “phi” patterns in Experiments 1, 2, (9) and Experiments 3-6, (9), respectively). Therefore, we conclude that the strain distribution in recurrent patterns does not result from material heterogeneities due to the model set-up, but that strain localization in the brittle layer controls the strain pattern and that deformation in the upper crust is effectively decoupled from the lithospheric mantle. Although the anticlines do not resemble periodic instabilities such as buckle folds, the driving mechanism may be similar; insofar that it is the strong brittle layer that controls and initiates the structures (e.g., Martinod and Davy, 1994).

The decoupling layer in the models is usually the lower crust; in experiments with a low-viscosity layer decoupling takes place higher up in the lower crust, along this additional horizon. Decoupling occurs only within the weak domain and not within the vises, as they do not deform significantly internally.

### 7.3.4. Reproducibility of experiments

The general evolution of the strain pattern can be reproduced when the same experiment run is repeated or even when second order features are varied (i.e., an additional decoupling horizon or a different strength contrast), as it is the case for experiments 4, 5, and 6. Yet, they have a comparable aspect ratio of structures. In this regard, the general distance between e.g., the anticlinal hinges is alike. Experiments also bear a close resemblance when compared with results from other analogue studies. In general, we do not aim to reproduce the exact position of every single thrust, the number of thrusts or the same timing of deformation, but the orogen scale pattern and associated aspect ratios of structures.

The cross-shaped pattern occurs in experiments by Cruden et al. (2006), in which case the system has open sides to allow for lateral extrusion. Yet, the aspect ratios and angles between structures of the “cross” are very similar. Also, experiments by Cagnard et al. (2006) exhibit a “phi” pattern, although they use a velocity discontinuity to localize strain in the center of the model. Still, the final pattern exhibits curved structures (anticline/syncline structures), that leave an undeformed area in between.

## 7.4. Parameter effect

### 7.4.1. Vise geometry

We tested both straight and curved vises (convex vise at the piston wall, concave vise on the opposite side) with a curvature angle of 20°. This curvature determined both the location and orientation of the faults, which typically form step-over zones. With straight vises, strain localizes along faults that develop from the boundaries close to the piston further inwards to the center, and moves again to the sides close to the opposite wall. The resulting pattern is “cross-shaped” (e.g., Exp. 1 and 2, Fig. 7.5a+b). With curved vises, the orientation of the step-over zones is inverted: strain localizes first in the center close to the moving vise 1, then along faults stepping over to the sides, which step in again towards the center. This pattern resembles a horizontal “phi” (e.g., Exp. 3, 4, 5, 6). Figure 7.8 shows the relation between the finite strain pattern and the approximate stress field, that we assume for the corresponding geometries (cf., e.g., Eisbacher, 1996). The structures of the upper crust are



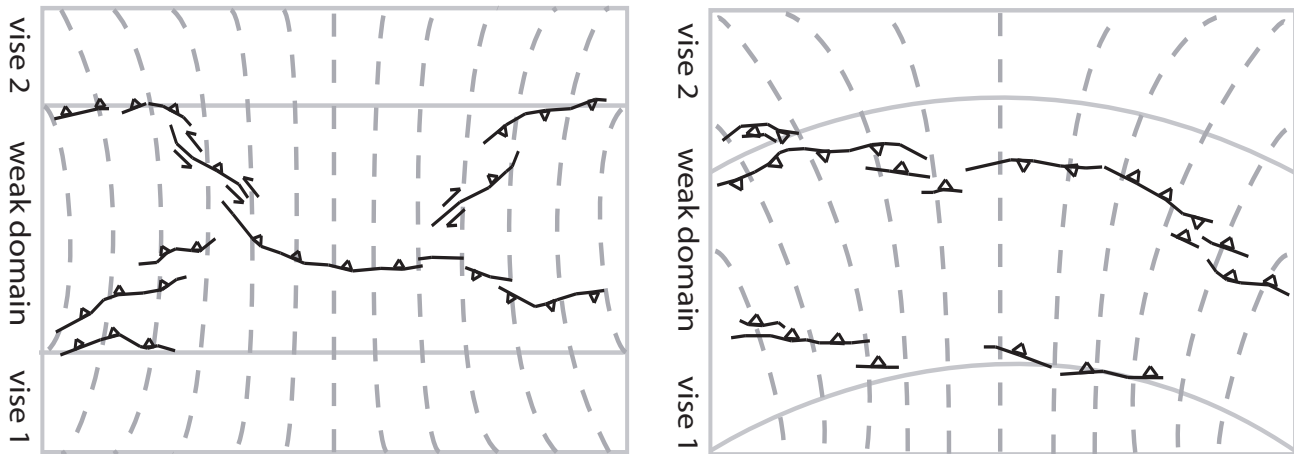


Fig. 7.8: Principal stress trajectories (dashed grey lines) approximately match the position of thrust/anticline structures in the upper crust (solid black lines), and thus explain the observed finite strain pattern: cross-shaped pattern for straight vise geometry (left) and “phi” pattern for curved vise geometry (right).

roughly perpendicular to the stress trajectories, so that the position of strain localization can readily be explained by the geometry of the vises.

If the geometry of the vises on either side of the weak domain is dissimilar/ asymmetric, both the position and orientation of faults change along-strike. Along the width of the small curved vise 1 in Exp. 7, the strain pattern resembles the “phi”-pattern. Beyond its width, the pattern is influenced by the straight geometry of vise 2, and changes from the “phi”-pattern to the “cross-shaped” pattern (Fig. 7.5g).

## 7.4.2. Strength contrasts

### 7.4.2.1. Horizontal strength contrasts

The lower crust is weaker than the mantle lithosphere, both within the vises and the weak domain. However, in most of our experiments the mantle lithosphere of the weak domain is thinner than the mantle lithosphere of the vises. Only in Exp. 1 and Exp. 6 do the weak and the strong mantle lithosphere have the same thickness (2 cm instead of 1 cm). The thickness of the layers has an influence on the integrated strength and therefore on the lateral contrast.

Experiments with relatively thick mantle lithosphere result in a wider final deformation pattern than other experiments. The anticlines are spaced much farther apart in Exp. 6 (Fig. 7.5f), than for instance in Exp. 4 (Fig. 7.5d) and Exp. 5 (Fig. 7.5e). Thus, the thickness (Exp. 1, 6) or in turn an increased horizontal strength contrast controls the spacing of the deformed zones, changing the pattern and position of strain localization, which becomes more widely distributed with increasing lithospheric thickness.

An additional low-viscosity layer enables decoupling (Exp. 5, Fig. 7.5e) at a higher level than in experiments without this layer, in which decoupling occurs in the weaker lower crust (e.g., Exp. 4). Depending on the position of the decoupling horizon, the crust below it undergoes pure shear, and does not participate in the anticline formation. Interestingly, the final orogen scale strain pattern is very similar, either with or without an additional decoupling horizon. This suggests that decoupling effectively takes place at similar depth in the lower crust when no additional decoupling horizon is introduced.

### 7.4.2.2. Lateral strength contrasts

In order to accumulate strain solely within the weak part of the lithosphere rather than within the vises, the vises must be stronger than the weak domain. Viscosity ratios between the strong and the weak equivalents in our experiments have values of about 2.2 for the lower crust, and 6.2 for the mantle lithosphere. These ratios are rather low, as the viscosities for both the weak domain and the vises are on the same order of magnitude, indicating a relatively small strength contrast between the weak domain and the strong vises. Yet, these ratios are sufficient to accumulate strain within the weak domain and not to deform the vises.

If no strength contrast is present between the vises and the intervening domain, the homogeneous material of the weak lithosphere should deform similarly to the experiments of Martinod and Davy (1994), in which periodic instabilities (buckling) occurred simultaneously throughout the model. The thrust pattern observed

in experiments by Cagnard et al. (2006) also resembles ours, although they used a velocity discontinuity to initiate strain localization in the center of their experiments.

#### 7.4.2.3. Length of structural units

If the length of the weak domain is reduced, the potential area for strain accumulation becomes smaller, and it is likely that only one structure will develop in the center, even with non-buoyant crust (cf. Section 7.4.2.2.). Sufficient initial space is therefore needed to accommodate at least two anticlinal hinges that can preserve a basin, which is necessary for plateau initiation. Willingshofer et al. (2005) included a weak zone that had a length/thickness ratio of 3.34 (10:3) and 4 (10:2.5). In neither case was a basin captured for plateau initiation. In our experiments, the length/thickness ratio for the buoyant area in Exp. 9 (Fig. 7.5i) was 4.54 (10:2.2). In all other experiments, the length/thickness ratio was much higher, between 7.5 (24:3.2, Exp. 1+6, Fig. 7.5a+f) and 10.9 (24:2.2, all other experiments). The critical length of the structural unit is dependent on the thickness, which determines the integrated strength of the weak domain. The critical length/thickness ratio for the weak unit must be above a value that lies between ~5 and 7.5. We cannot exclude that, for basin capture to occur, this value is further coupled to the ratio of total length of the set-up and to the width of the units. In our experiments, the weak domain makes up 63% of the total length of the set-up, compared to 100% in Cagnard et al. (2006), who did not employ stronger vise blocks. In contrast, the weak zones in Willingshofer et al. (2005) comprised only 25% of the total length.

If the accommodation space is too small, material could also thrust over the vise blocks (“water bed effect”, Cruden et al., 2006), which themselves would bend downwards beneath the weak domain.

#### 7.4.3. Buoyancy

Two strong end members are used for the density of the lower crust to better evaluate the effect of buoyancy. We are aware of the fact that their densities are rather high (non-buoyant case) or rather low (buoyant case), when scaled back to nature (cf. Table 7.1).

When the lower crust is buoyant it tends to bulge upwards due to density inversion. This behaviour promotes strain localization in the

upper crust, which occurs at early stages of convergence (e.g., after 5% of bulk shortening, Exp. 2, 3), whereas strain localization in the upper crust typically does not start until about 12% of bulk shortening in non-buoyant experiments (with 27.7% being the total amount). Also, the mode of strain accumulation within the viscous layers is different: with a buoyant crust, homogeneous thickening dominates in the mantle lithosphere, whereas with non-buoyant crust thickening occurs in the weak lower crust.

In general, the effect of a buoyant lower crust is to enhance strain localization in fewer structures, which are positioned within the center of the weak domain. Non-buoyant crust tends to localize strain along numerous thrusts, which are more distributed and have wider spacing (viz., Cruden et al., 2006). This is particularly well observed in Exp. 9 (Fig. 7.5i), where one area of buoyant lower crust is located in between two non-buoyant lower crustal domains. Here, the structure develops in the middle of the buoyant area. It extends almost perfectly perpendicular to the direction of compression, thereby remaining in the buoyant domain. Similarly, the cross-shaped pattern in Exp. 1 (non-buoyant lower crust, Fig. 7.5a) occurs over a wider area than for example in Exp. 2 (buoyant lower crust, Fig. 7.5b), in which deformation localized on a smaller area.

In order to initiate the formation of a plateau, deformation must localize not only at one dominant structure in the center, but along two or more structures that entrap an intervening basin. This is only possible when the crust is non-buoyant. This counterintuitive result reflects the importance of the buoyancy on the timing and location of strain accumulation for plateau initiation.

#### **7.5. Comparison of three experiments with plateau-initiation**

In the following, we compare characteristics of the three experiments that exhibit basin capture and plateau initiation (Exp. 4, 5, 6), and examine the along-strike variation of the orogen scale pattern, i.e., differences on the suborogen scale.

In all plateau-style settings (Fig. 7.9a+b), the model possesses a non-buoyant, weak lower crust and a sufficient strength contrast between the curved vises and the weak domain (viscosity ratios between the strong and the weak mantle lithosphere are around 6). Exp. 4 (Fig. 7.5d) is referred to as the “basic setting”, Exp. 5 (Fig.

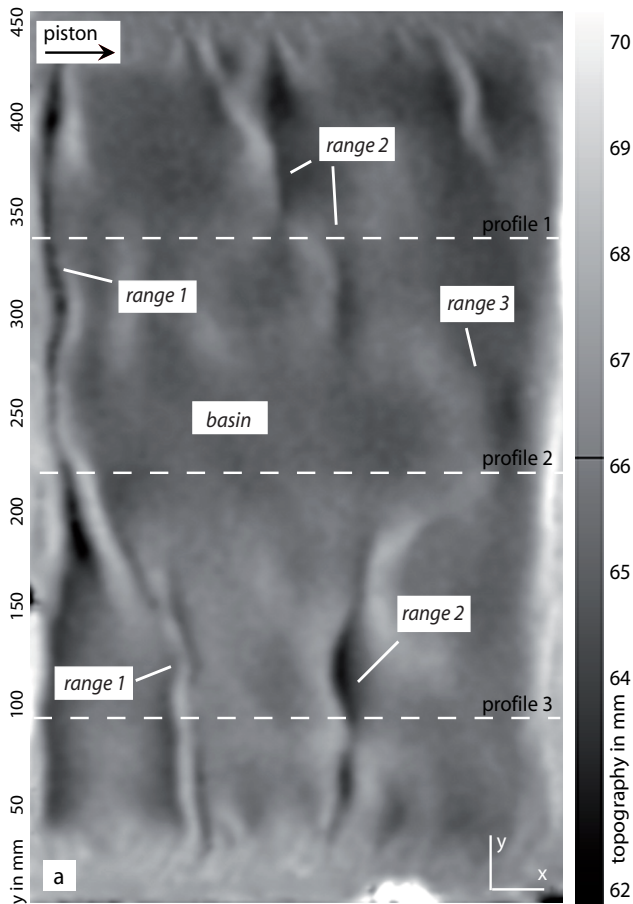


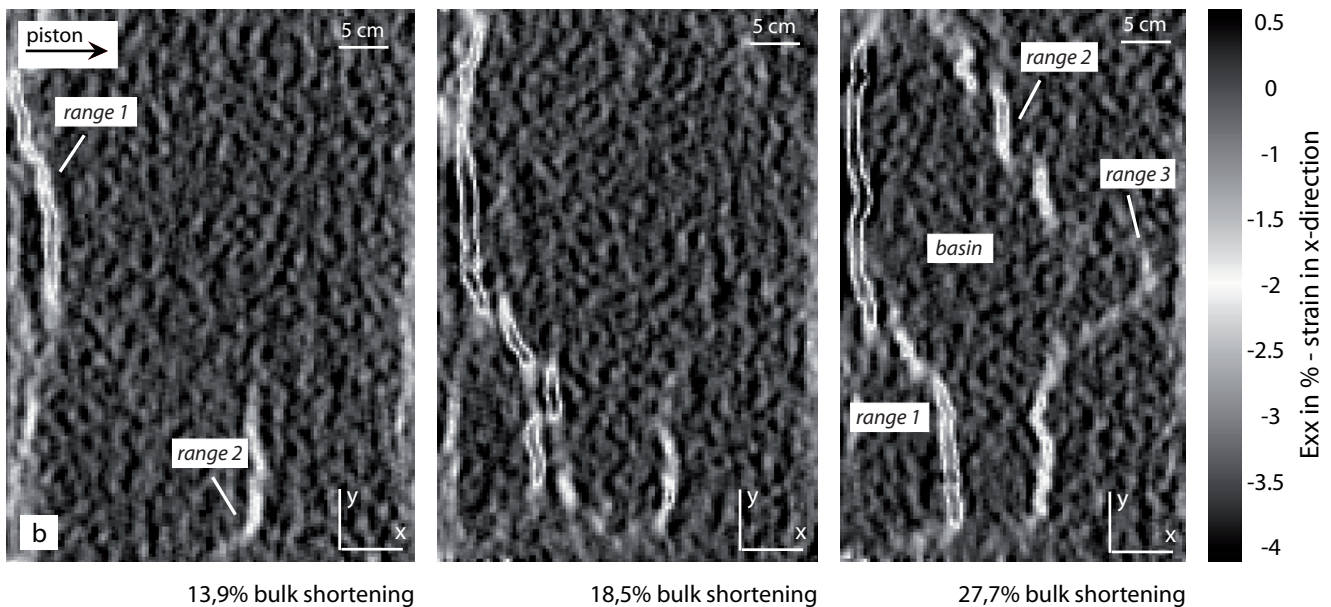
Fig. 7.9a (top), b (bottom): a) Topography of the final surface of Exp. 4 after 10.5 cm of convergence as recorded by PIV. Light colours indicate high elevation, dark colours subsided areas. Both anticlinal ranges (range 1 and range 2) bounding the basin area are delineated by elevated thrusts/anticlines (white). The initial surface was at a height of 63 mm. White dashed lines depict location of three profiles. b) Strain accumulation (% of strain in x-direction) of Exp. 4 as recorded by PIV. Light colours outline regions of high strain. Thrusting in the upper crust starts at ~11.5% of bulk shortening, and two peaks (range 1 and range 2) develop that bound an undeformed area (basin).

7.5e) has an additional low-viscosity layer (“LVL setting”), and Exp. 6 (Fig. 7.5f) has a thick weak mantle lithosphere (“thick setting”).

In all three settings strain is accumulated by thrusts within the upper crust, cusp-shaped hanging wall anticlines bounded by deep synclines in the weak lower crust (Fig. 7.7), as well as thickening of both the lower crust and the mantle lithosphere. The vises themselves remain undeformed. For the three plateau-initiation settings, we further describe differences in 1) time series of strain accumulation at the surface (Fig. 7.10), 2) topographic profiles orthogonal to the weak domain (Fig. 7.11a+b), and 3) the finite strain accumulation within the viscous layers (Fig. 7.12). The location of the profiles is marked in Figure 7.9a, and is the same for each of the three experiments.

### 7.5.1. Differences in plateau style: strain distribution profiles

The three plateau-initiation settings display pronounced differences in strain evolution. High strain accumulation is coloured black. Thrusts are pointed at by little arrows. Fault zones in the “basic setting” are narrow and discrete, with a spatially homogeneous strain accumulation (Exp. 4, profiles 1 to 3, Fig. 7.10). In contrast, the “LVL setting” has wide fault zones, which have a diffuse margin around a dominantly accumulating core (Exp. 5, profiles 1 to 3, Fig. 7.10). Even more diffuse are the fault zones of the “thick setting”, with small dominant cores that are surrounded by areas of reduced strain accumulation (Exp. 6, profiles 1 to 3, Fig. 7.10). This probably occurs because more strain can be accumulated within the thicker





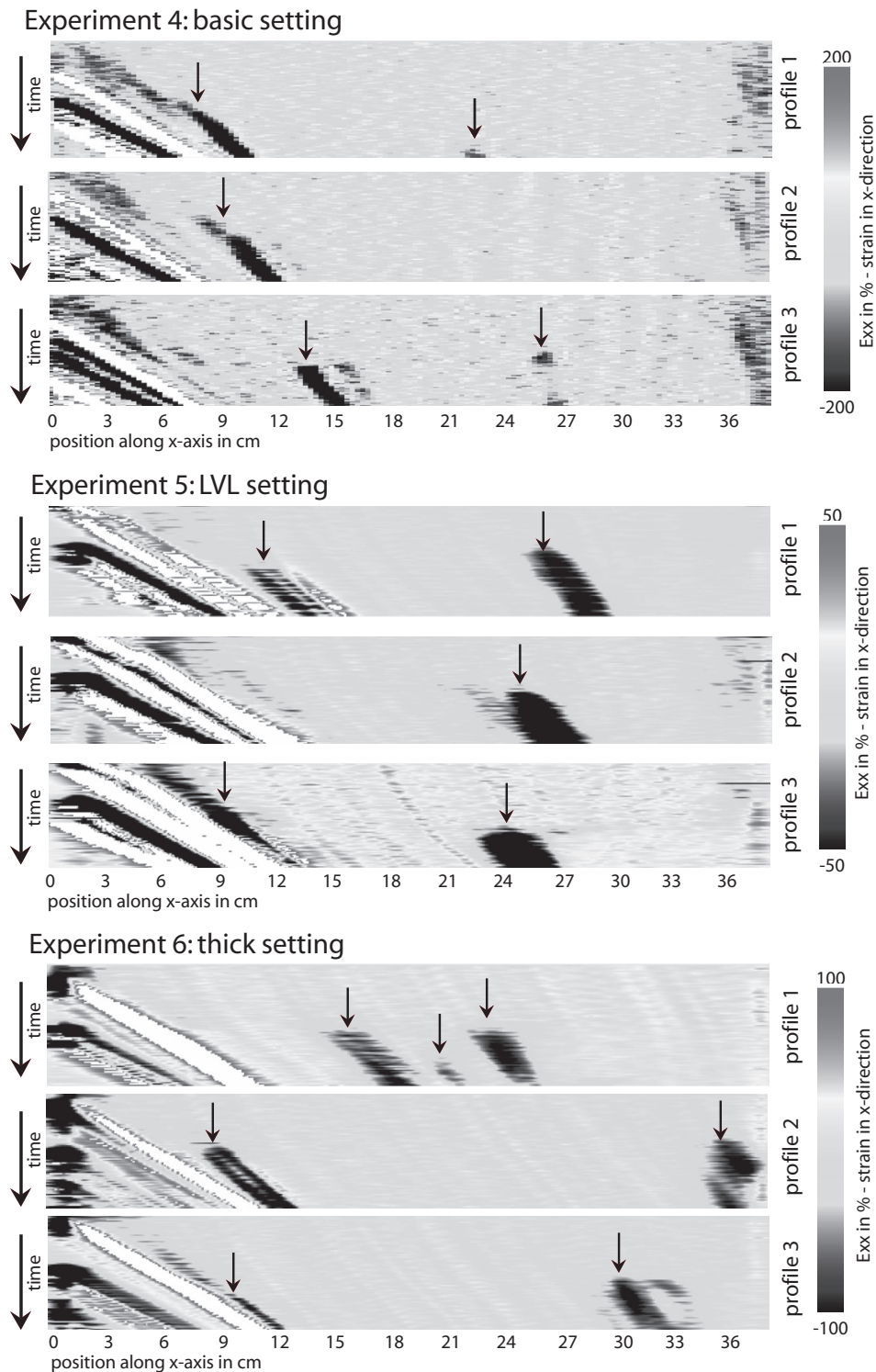


Fig. 7.10: These time series through plateau-initiation settings (Exp. 4, 5, 6) show strain data along profiles crossing the surface area similar to the strain surfaces of Figure 7.9b. The profiles for each time step are plotted below each other, so that the figures are read from top to bottom as time increases. Convergence increases from left to right; thus the motion of the piston is reflected by the oblique white patch with respect to the position along the x-axis. Dark colours depict fault zones with very high strain accumulation (Exx), indicated by small arrows. Depending on the position of structures, we can infer both the temporal and spatial (along a profile) strain accumulation within one experiment. Further explanation in-text.

mantle lithosphere.

In general, all of these settings develop two main thrusts (which bound the basin area) in which strain accumulates. In the basic setting, the first thrust close to the piston accumulates more strain than the second. The latter accumulates

strain in discontinuous pulses (interruption of “black” high strain periods by “light” low strain periods). A similar but less pronounced effect can be observed in the LVL setting, in which the second thrust is more dominant. The thick setting does not contain a dominant structure, but strain

## 7. The effect of mechanical heterogeneity on plateau initiation

accumulation switches back and forth between the two main thrusts. In general, both thrusts appear to accumulate the same amount of strain (e.g., Fig. 7.10, profile 1, Exp. 6).

“Secondary” faults also occur in both the basic (Exp. 4, profile 2) and the thick setting (Exp. 6, profiles 1 to 3). These are faults that are located “behind” another fault and accumulate less strain

than the main faults closer to vise 1. In the thick setting secondary faults are more pronounced and also more diffuse in both geometry and timing of strain accumulation.

The spacing of the main thrusts differs along-strike. In general, the spacing is narrower in the basic setting than in the LVL setting. This can be attributed to the fact that the LVL is a

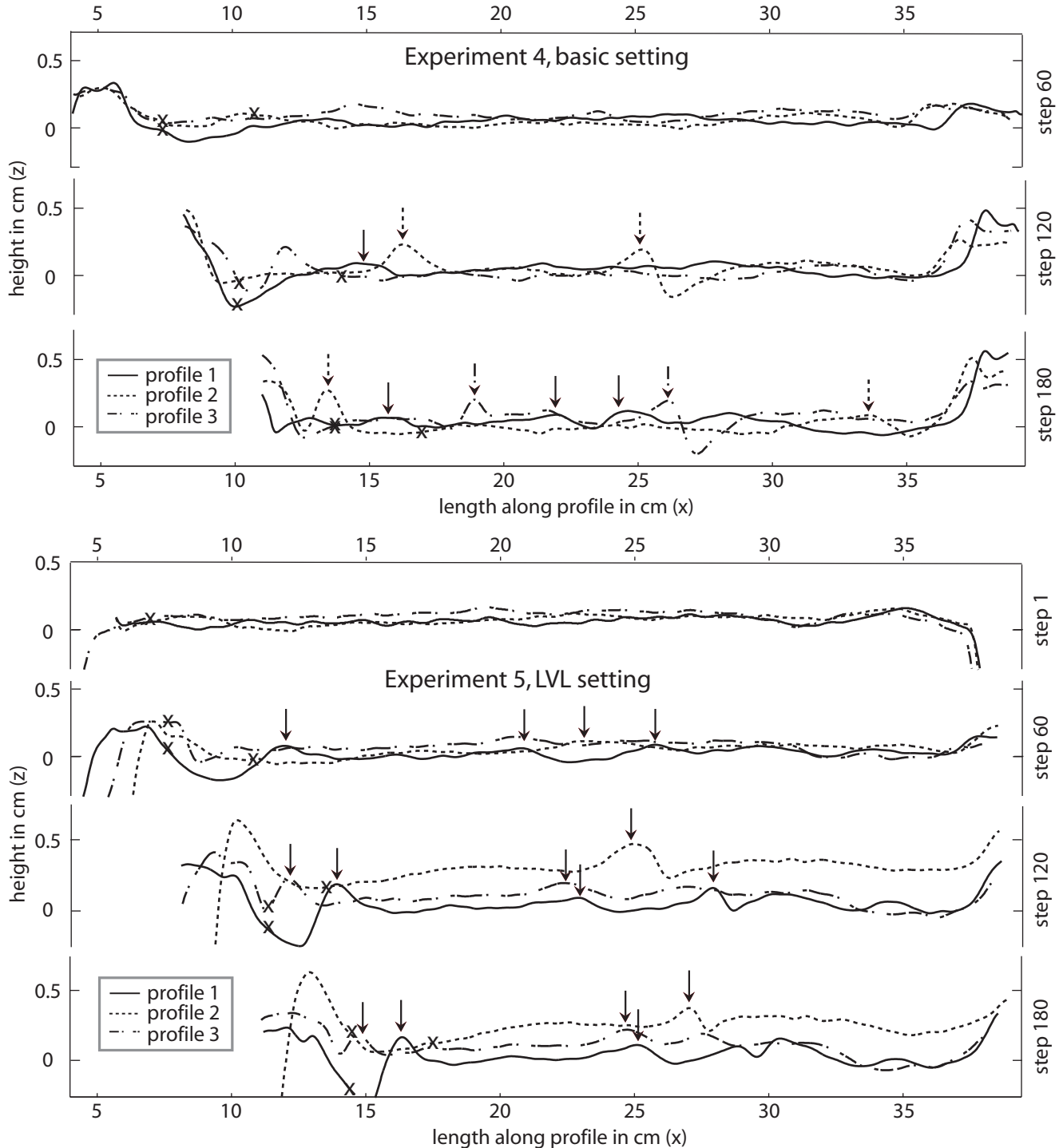


Fig. 7.11a (top), b (bottom): a) Topographic profiles of the basic setting. For each of the three profiles of Exp. 4 (location in Fig. 7.9a), three time steps are shown (60, 120, and 180 equaling 9.2%, 18.5% and 27.7% of bulk shortening). Further explanation in-text.

b) Topographic profiles of the LVL setting (Exp. 5). The four time steps (60, 120, and 180 equaling 9.2%, 18.5% and 27.7% of bulk shortening) are depicted together for all three profiles (profiles 1, 2, 3; location in Fig. 7.9a). Crosses indicate the approximate position of the boundary between vise 1 and the weak domain. Arrows point to the main anticlinal hinges.

decoupling horizon weaker than the “basic” lower crust allowing coherent displacement of wider thrust sheets towards the foreland.

Pronounced differences do not only occur from one experiment to the other, but within one setting. In this regard for example, both the number and position of primary and secondary faults change along-strike in the “thick setting”, and thus also the spacing and the amount of strain accumulated by individual faults. The spacing is either very small (Exp. 6, Fig. 7.10, profile 1) close to the sides, or very large in the center (Exp. 6, Fig. 7.10, profile 3).

### **7.5.2. Differences in plateau style: topography**

The topographic evolution is strongly linked to the strain evolution, as thrusts and anticline-syncline structures typically represent areas of local relief. Thus, the above differences in strain evolution along-strike within one experiment also apply to the development of topographic relief. Figure 7.11a plots differences in topography for the basic setting; in profiles 1, the main ridges are widely spaced whereas they are closer together in profile 3.

The initiation of topography development coincides with strain localization. The spacing of topographic features in the LVL setting (Fig. 7.11b) is more or less constant along-strike. This occurs although the elevation of the area between the main ridges differs. The undeformed areas crossed by profiles 2 and 3 (Fig. 7.11b) have experienced uplift, whereas profile 1 has experienced subsidence with respect to the initial surface. In general, subsidence of the undeformed areas is common, which is part of the plateau-initiation process.

### **7.5.3. Differences in plateau style:**

#### **3D thickening of the lithosphere**

About ten cross sections were made of each experiment (five inward from each side in 2-3 cm steps) and the thicknesses of both the lower crust and the mantle lithosphere of the weak domain were measured. The change in thicknesses are plotted and contoured in Figure 7.12. When plotted on top, structures in the upper crust roughly bound areas of homogeneously thickened viscous layers. In general, the location of pronounced thickening is similar in both the lower crust and the mantle lithosphere, with local deviations where a low in the mantle lithosphere coincides with a region of increased thickness of the lower crust (e.g., Fig.

7.12, Exp. 5, LVL setting).

The amount of strain that is accumulated in the different layers varies: in the basic setting (Fig. 7.12, Exp. 4), depending on the location, the initial thickness of the mantle lithosphere increases by 50-100%, and of the lower crust by 10-20%. This is similar in the thick setting (Fig. 7.12, Exp. 6), where the mantle lithosphere has increased by 50% and the lower crust by 10-20%. In contrast, the LVL setting (Fig. 7.12, Exp. 5) has experienced only a 25-50% increase in mantle lithosphere thickness, and between 10% of thinning (first half of the weak domain, closer to vise 1) to 10% of thickening in the lower crust (in the second half towards vise 2). This can be attributed to the fact that the LVL acts as a decoupling horizon at a high level within the lower crust. The material within the lower crust below this horizon does not accumulate much strain. Therefore, the volume of material that can thicken is less than in the other plateau-initiation settings, and is mainly restricted to the volume above the decoupling horizon.

The location of crustal thickening is also dissimilar for the three models. In the basic setting (Exp. 4), the thickness decreases away from the piston. In the LVL setting (Exp. 5), strain is accumulated in the far half of the weak domain, closer to vise 2, which again can be explained by the decoupling layer within the lower crust.

In the mantle lithosphere of the thick setting (Fig. 7.12, Exp. 6), strain accumulation is most pronounced at the boundaries with the vises. This suggests that the lithosphere is likely to thicken closer to the boundary of the weak domain and the vises, i.e., the mechanical anisotropy, when the strength contrast is low. When it is high, viscous layers thicken more homogeneously in the center of the weak domain, as is the case for the LVL setting.

## **7.6. Discussion**

### **7.6.1. Parameter control**

Plateau initiation includes the formation of at least two mountain ranges that are separated by an undeformed area (e.g., Fig. 7.9a+b), which is a basin prone to undergo sedimentary infill due to internal drainage resulting in surface uplift (e.g., Meyer et al., 1998; Sobel and Strecker, 2003; Sobel et al., 2003) (cf. Fig. 7.1). Typically, such mountain ranges do not form in fold-and-thrust belts where one range develops close to and after another as strain and evolving thrusts propagate

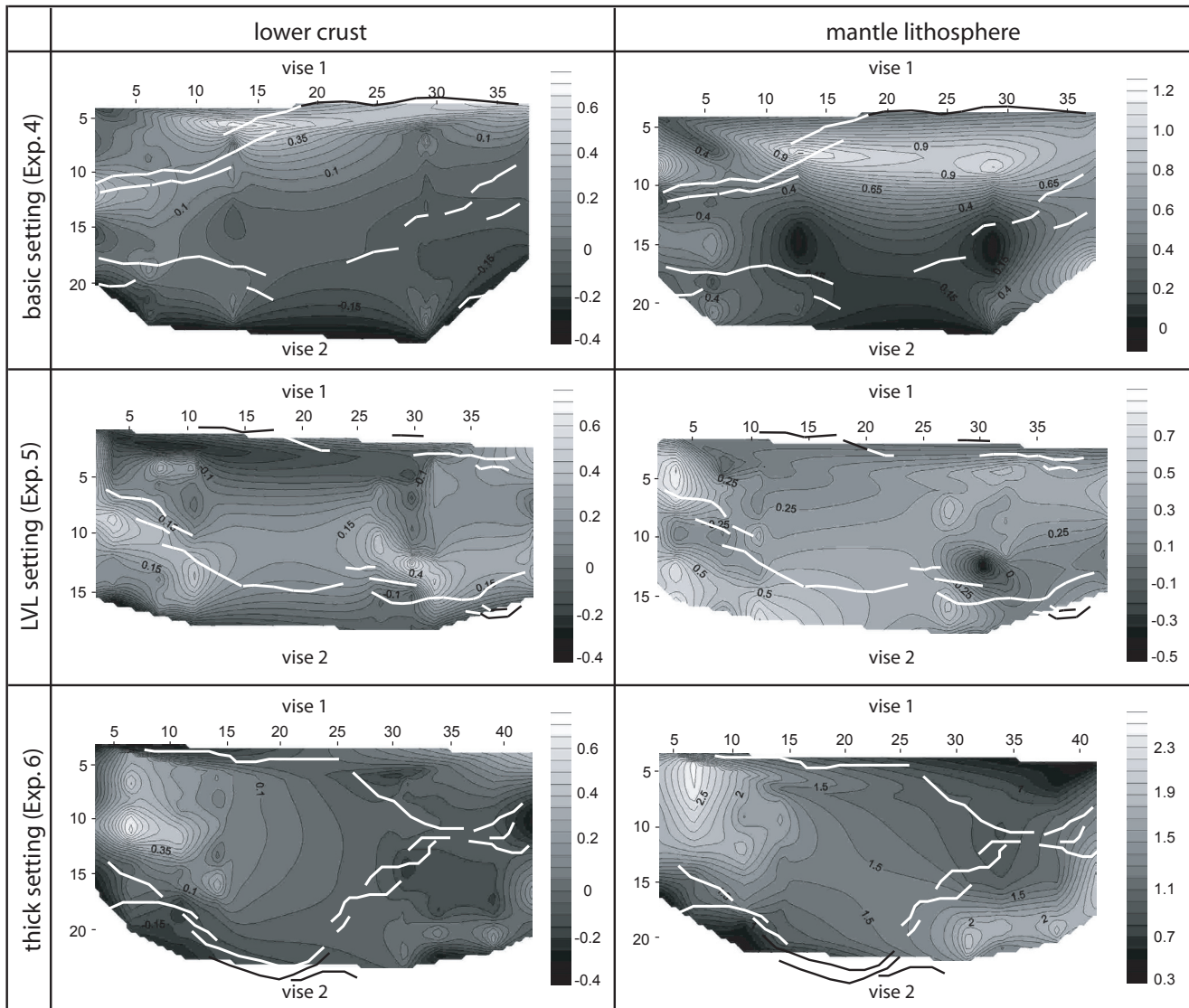


Fig. 7.12: Increase in thicknesses of viscous layers in centimetres (left: lower crust, right: mantle lithosphere) for the three plateau-initiation settings (top: basic setting (Exp. 4), centre: LVL setting (Exp. 5), bottom: thick setting (Exp. 6)). Note that colour palettes differ slightly for each of the figures. Structures (thrust/anticlines) of the upper crust are marked with white and black lines. Further description in-text.

towards the foreland, and hence do not leave enough accommodation space for basin infill and do not in general produce plateaux. In contrast, decoupling of deformation in the upper crust from the lower crust or the upper mantle reduces frictional resistance at the base of the upper crust and, hence, allows displacing longer coherent slabs before their strength limit is reached, which is the key prerequisite for plateau initiation.

The initial strain pattern required for subsequent plateau growth only occurs when all of the following parameter conditions are met:

1. The vertical layer density stratification must be gravitationally stable (non-buoyant crust with respect to the upper crustal parts) to enable strain localization with spacing several times the thickness of the upper crust.
2. A lateral strength contrast between the

strong portions of lithosphere enclosing a weaker part must be present.

3. The lateral contrast between the weak domain and the vises must be sufficient to localize strain solely in the weak domain. If it is too strong the whole weak domain buckles at once, with the first buckle localizing close to vise 2, in which case only one anticlinal range develops with no entrapped proto-basin (see Willingshofer et al., 2005).

4. The weak domain must be long enough to allow strain accumulation in two locations. The critical threshold for the length/thickness ratio is above a value between  $\sim 5$  and 7.5.

5. The geometry of the strength contrast must be curved for both vises (convex vise 1, concave vise 2) to enable the localization of two laterally linked anticlinal ranges that enclose



accommodation space for an intervening basin. With reduced curvature and in an open system, the width of the deformational system could in principle grow to very large values, precluding the trapping of closed basins. This probably occurs with length-width ratios  $<0.6$  (e.g., Exp. 1 and 2, and experiments by Cruden et al. (2006), which allow lateral extrusion).

Although a lack of buoyancy of the lower crust appears as a necessary condition (1. point) for a basin area to be entrapped between the anticlines, such an area also develops with buoyant lower crust and curved visé shape (Exp. 3), but it is very narrow. The next three points above (2-4.) hold for all of the experiments. Yet, two different strain patterns (the “cross-shaped” and the “phi”) can be distinguished, which depend solely on the geometry of the lateral strength contrast. As it has not been demonstrated if the cross-shaped pattern can develop captured basins in a larger experimental set-up, we assume that the most crucial parameter in our experiments for the development of a strain pattern that enables subsequent plateau initiation is the curvature of the visés. The geometry of the visés changes the corresponding stress field, whose stress trajectories roughly match the position of structures of the upper crust (which are perpendicular to the trajectories, Fig. 7.8) and can therefore explain the resulting finite strain patterns.

The spacing between anticlinal hinges is influenced by the thickness of the weak domain. If the lithosphere is thicker (e.g., similar thickness of weak and strong crust, Exp. 6), fold hinges are farther apart than when the lithosphere is only half the thickness of the visés. This effect is similar to spacing relations in the upper crust (e.g., Mulugeta and Koyi, 1992; Koyi, 1995; Morellato et al., 2003), which depend on the thickness of the deformed layer, and also on the basal and internal friction of the layer. The latter can be regarded equivalent to the integrated strength of the units. Unlike typical fault spacing in e.g., fold-and-thrust belts, the spacing between the anticlinal hinges in plateau initiation settings varies along-strike: the maximum distance between the anticlinal hinges is typically in the center, which decreases towards the sides, so that the captured basin is “closed off” (cf. Fig. 7.5d-f).

### 7.6.2. Application to the Andean plateau

The Central Andean plateau comprises

four main structural units from west to east: the Western Cordillera, the highly elevated plateau area (Altiplano-Puna), the Eastern Cordillera and the Subandean fold-and-thrust belt (Fig. 7.2). The main characteristics on the orogen scale are two mountain ranges (the Cordilleras) that bound the flat and rather undeformed plateau area in between (e.g., Isacks, 1988). External to this “orogenic system” is the fold-and-thrust belt, which formed once the plateau had become stable (e.g., Allmendinger and Gubbels, 1996).

When looking at scales smaller than the orogen itself, we observe flat and undeformed areas that are bounded by adjacent ranges (Fig. 7.2) similar to our experiments. These undeformed areas are not necessarily plateau areas yet, but rather marginal basins that are in the process of being internally drained (e.g., in the Puna: Sobel and Strecker, 2003; Sobel et al., 2003). After “regional” plateau initiation, these features are incorporated into the “orogenic-scale” plateau (e.g., Mortimer et al., 2007). Thus, some of these basins are not yet at the stage of attaining a highly-elevated plateau region, but are still in the plateau-initiation phase, as e.g., for the Sierras Pampeanas region. Subsequently, the area will internally drain, uplift and be filled with sediments, and thus be incorporated as “regional” plateau areas in the orogenic plateau of the Puna.

Our experiments resemble these plateau initiation settings, in which two ranges allow the preservation of a peneplain, which may undergo basin-like subsidence or uplift. The topographic relief in our models is unrealistically high when scaled back to nature, but this is due to the lack of erosion. Therefore it is likely that significant amounts of debris from adjacent ranges can produce the infill for the initial basin in our models as observed in the northern Sierras Pampeanas in Argentina (Sobel and Strecker, 2003), if we were to model erosional processes with tectonic river cut-off and internal drainage.

Critical parameter combinations must be met early on in the system for a plateau-style system initiation, which includes a normal crustal density profile, a lateral strength contrast with a critical curvature (the hot back-arc region is compressed between the strong and cold “pseudo-indenting” fore-arc to the west (Victor et al., 2004; Tassara, 2005) and the thick cold Brazilian shield to the east (e.g., Sobolev and Babeyko, 2005), both with curved in-plane geometries, see Fig.

7.2), a decoupling horizon within the lower crust (a zone of partial melt or weak lower crust beneath the Altiplano-Puna plateau; Yuan et al., 2000), and a sufficient initial width. Isacks (1988), Kay and Kay (1993) and Allmendinger et al. (1997) have all proposed that thermal weakening of the crust or delamination of the mantle lithosphere are necessary prerequisites of plateau formation.

The fact that we observe variations in strain partitioning mode, topographic relief and the extent of peneplains on several scales below the orogen scale in our models, emphasizes the observation that internal basin drainage and plateau initiation occurs on scales ranging between 400 km (e.g., for the Altiplano basin) down to scales <100 km (e.g., smaller basins in the Puna and the Sierras Pampeanas, cf. Fig. 7.2). Also, it reproduces local along-strike differences in, for example, elevation or spacing of structures.

### 7.6.3. Previous modelling studies

Most modelling studies focus on the effect of one parameter on the formation of a plateau -and not the plateau initiation- (e.g., thermal perturbation within the lithosphere (Wdowinski and Bock, 1994a+b); crustal flow (Royden 1996), gravity-driven channel flow (Husson and Sempere, 2003), flow indentation of the lower crust (Gerbault and Willingshofer, 2005), mass flux along a detachment (Vietor and Oncken, 2005)), rather than the influence of coupled parameters (e.g., the combined influence of crustal thickness and interplate friction, Sobolev and Babeyko, 2005). Analogue experiments by Schemmann and Oncken (under review) are the first to reproduce not only e.g., the final stage of the plateau-style setting, the finite strain pattern or the topographic evolution, but the development of orogen scale deformation in time and space for the Central Andean plateau, as well as the strain evolution of single faults of the structural units. This requires that two parameters of mechanical heterogeneity are coupled (namely internal and basal strength contrasts), for which Schemmann and Oncken (under review) pinpoint critical threshold values. These determine the deformational type that will form, i.e., a plateau-style or a wedge-like system.

One of the advantages of their analogue set-up is the implementation of granular media. This allows the successive test of different materials to precisely set the limits for critical threshold values without changing the stress scaling factor. At the

same time, modelling only the brittle upper crust without taking isostatic effects (e.g., buoyancy) into account, as well as decoupling the crust from a stiff base, imply limiting boundary conditions.

This study compensates for previous shortcomings by employing viscous and brittle media in a 4-layer set-up that accounts for more complexity similar to nature, dynamic scaling, pure and simple shear, and more effects such as strain rate and isostasy etc. Thus, more parameters than only two can be coupled (e.g., strength contrasts (internal and basal), buoyancy effects, lithospheric thickness, and plate geometry).

Schemmann and Oncken (under review) are able to resolve below the orogen scale, namely single faults in each structural unit. However, plateau formation was active only on the orogen scale. In contrast, this study can show that the same process, namely plateau initiation, is active on the orogen scale but at the same time also on scales below. In addition, we can examine the effect not only of first order features on scale related deformation and its variation but of second order parameters as well. These variations can be analyzed in the strain evolution, the development of topography and the finite crustal thickness.

### 7.7. Conclusions

Through 4-layer brittle-viscous analogue experiments, we conclude that the development of plateau-style settings only begins when the starting conditions follow a parameter combination that includes a critical lateral strength contrast between the strong bounding blocks and the intervening weak domain (the strength of the strong units should be at least twice the strength of the weak equivalent, but likely not more than ten times), a curved geometry of the vise blocks (convex vise 1 and concave vise 2), a decoupling horizon within the lower crust of the weak domain, and a non-buoyant lower crust.

Anticline-syncline structures and thrust faults that develop at their inflection points occur in all experiments. However, the necessary distance between the structurally controlled topographic ranges required for the preservation of an enclosed peneplain is only possible under the above conditions. This scenario can subsequently be subject to internal drainage, which is the next condition to the formation of a plateau. If we increase the thickness of the mantle, the surface pattern predicts even wider spacing of active

structures bounding basins and hence wider plateaux.

Along-strike of the main ranges, variations in strain evolution, topography and finite crustal thickness occur not only within one experiment, but also when comparing the three different plateau-initiation settings. This suggests that basin capture between tectonically active structures occurs at several scales, similar to small-scale basins in the Sierras Pampeanas (e.g., Sobel and Strecker, 2003, Mortimer et al., 2007) or larger basins like the Altiplano basin.

#### *Acknowledgments*

This work is part of KS' PhD thesis, funded by a grant from the "Studienstiftung des deutschen Volkes" (National Merit Foundation), who additionally sponsored her research visit to the Tectonophysics Laboratory at the University of Toronto. ARC acknowledges funding from the National Sciences and Engineering Research Council of Canada.